Transport Theory for Cationic Zeolites: Diffusion of Benzene in Na-Y

Scott M. Auerbach,*,†,∥,⊥ Neil J. Henson,‡,∥ Anthony K. Cheetham,†,‡,∥ and Horia I. Metiu†,§

Departments of Chemistry, Materials, Physics, and the Materials Research Laboratory, University of California, Santa Barbara, California 93106

Received: January 5, 1995; In Final Form: April 28, 1995⊗

We have modeled benzene diffusion in Na-Y zeolite (Si:Al = 2.0) over the temperature range 100−500 K. We apply the kinetic Monte Carlo random walk model, with activation energies derived from a new zeolite−hydrocarbon potential energy surface (PES). An Arrhenius fit yields the apparent activation energy $E_a = 41$ kJ mol^{-1}, as compared with the previously determined experimental values 14−27 kJ mol^{-1}. Minimum energy paths from the new PES demonstrate "cartwheel" and "skateboard" hopping mechanisms for benzene in Na-Y. Analysis of the results suggests that activation energies from long length scale diffusion measurements, e.g. pulsed field gradient NMR, should be interpreted as site-to-window activation energies, whereas those from short length scale experiments, e.g. spin−lattice relaxation NMR, correspond to intracage site-to-site activation energies.

I. Introduction

The structural, thermochemical, and dynamical properties of adsorbed hydrocarbons play a central role in catalytic processes that take place within the cavities of zeolites and other shape-selective, microporous catalysts. Selectivity, for example, may be strongly influenced by the diffusivities of reactant and product molecules. Computational studies have made a significant impact in this area during the last 10 years, helping to elucidate zeolite framework structure,[1] hydrocarbon adsorption,[2,3] sorbate dynamics,[4] and catalytic activity.[5,6] Molecular dynamics (MD) simulations have been particularly useful in modeling rapid diffusion in zeolites. However, in many important examples, such as cationic or acidic zeolites, MD cannot be used because the molecules are trapped at binding sites with long residence times. In such cases the kinetic Monte Carlo (KMC) algorithm is the method of choice for modeling diffusion and indeed has been used extensively to study surface growth[7] and adsorption.[8] Although KMC has been applied to low-temperature diffusion of Xe and SF_6 in silicalite,[9] no simulation of transport in technologically useful zeolite systems has been reported. Here we use KMC to model benzene diffusion in Na-Y (Si:Al = 2.0), a synthetic faujasite, focusing on the microscopic factors which control short- and long-range mobility.

The faujasite microporous structure naturally partitions benzene mobility into two length scale regimes.[10−14] Over length scales less than 1 nm, benzene executes intracage, site-to-site jumps which tend to randomize the benzene plane orientation. Site-to-site hopping rates have been measured by spin−lattice relaxation NMR experiments for benzene in a series of faujasites.[15] In addition, recent two-dimensional NMR exchange experiments for benzene in Ca-X (Si:Al = 1.0) have measured rates for site-to-site benzene jumps by exploiting their discrete angular nature.[16] Theoretical site-to-site activation energies have been reported for benzene in several cation-containing faujasites[17] and for various aromatics in Na-Y.[18] Over longer length scales, benzene executes a random walk through the zeolite by making cage-to-cage hops through window sites connecting adjacent supercages. The rate of these intercage jumps determines the intracrystalline diffusion coefficient, which can be measured by pulsed field gradient NMR. It is unclear whether the intercage jump rate is determined simply by a fundamental intracage jump or rather is a complicated mixture of many such rates. By using KMC to model long-range motion in terms of fundamental jumps, we determine the connection between short- and long-range mobility and hence provide a unified interpretation of the NMR experiments discussed above. For benzene in Na-Y at infinite dilution, we find that the benzene diffusion coefficient is determined simply by the site-to-window hopping rate.

The remainder of the paper is as follows: in section II we discuss the Na-Y−benzene potential energy surface, binding sites, and energies. In section III we describe the theory of activated diffusion and give details regarding the implementation. Section IV illustrates the fundamental hopping processes and calculates their activation energies. Section V analyzes the resulting diffusion coefficients for benzene in Na-Y, and in section VI we conclude.

II. Potential Energy and Binding Sites

A. Partial Charges. We have recently developed a new zeolite−hydrocarbon potential energy surface[19] (PES) which accurately reproduces the structure of the faujasite framework and that of the main benzene sorption sites, as determined by the powder neutron diffraction studies of Fitch *et al.*[20] These experiments, performed with 1.1 and 2.6 benzenes per supercage, have obtained the same two binding sites at both coverages. In the primary site, denoted as S_{II}, benzene binds to a Na ion coordinated to a zeolite 6-ring; the secondary site, denoted as W, involves benzene in the 12-ring window separating two adjacent supercages.

We model the zeolite−hydrocarbon system as a collection of partially charged ions interacting *via* short- and long-range forces. Our partial charge model deviates in philosophy from more standard formal charge models,[21] which have been shown to accurately reproduce crystallographically determined zeolite structures such as faujasite,[21,22] silicalite,[21,22] ferrierite,[22] and zeolite A.[21] They are also very convenient for introducing

* Author to whom correspondence should be addressed.
† Department of Chemistry.
‡ Department of Materials.
§ Department of Physics.
∥ Materials Research Laboratory.
⊥ Present address: Departments of Chemistry and Chemical Engineering, University of Massachusetts, Amherst, MA 01003.
⊗ Abstract published in *Advance ACS Abstracts,* June 1, 1995.

0022-3654/95/2099-10600$09.00/0

heteroatoms such as H^+,[23] Ge^{4+},[24] La^{3+},[25] and Ti^{4+} [26] into zeolite frameworks. However, because the zeolite frame is largely covalent, as demonstrated by quantum cluster calculations,[27,28] the use of formal charges overestimates Coulombic forces, requiring compensating errors in other parts of the PES. There is no guarantee that this cancellation of error will occur for geometries other than the one used for fitting. Thus, with the intent to model both stable and activated host−guest structures, we use a more physically plausible partial charge model.

We replace Si and Al atoms with an average tetrahedral-site atom (T-atom) because of the difficulty in experimentally determining Al distributions in disordered zeolites. The charge on the average T-atom is determined by averaging Si and Al partial charges, according to the Si:Al ratio being considered. This approximation has been used in most molecular mechanics simulations of disordered zeolites. However, recent evidence[29] of Al and Si layering along the (111) plane in faujasite suggests that the average T-atom model may underestimate diffusive length scales and may totally neglect diffusive anisotropy. As more evidence characterizing Al distributions becomes available, it may be important to develop theoretical methods which relax the average T-site approximation.

We assume a Si:Al ratio of 2.0, hence zeolite Y, requiring 64 Na ions per unit cell to balance charge. We assume full occupation of Na sites I′ (32 per unit cell, located in smaller β cages) and II (32 per unit cell, located in supercages). This occupancy model is reasonable considering that only the Na(II) ions are accessible to a penetrant the size of benzene. In addition, diffraction studies of Na-Y (Si:Al = 1.7) find nearly full Na(II) occupation.[30]

Our general approach to fitting this potential involves fixing the charges and fitting the remaining short-range potential parameters to reproduce crystallographic and thermochemical data (for more details please see ref 19). As such, we are guaranteed to reproduce the faujasite structure, in addition to the structure and binding energy of benzene in its most stable sorption site. The question remains whether we can use this PES to generate reliable hopping activation energies for benzene mobility. We show below that this procedure is indeed capable of giving qualitatively reasonable transition state energies.

B. Functional Form and Potential Parameters. We now discuss the potential energy of a Na-Y (Si:Al = 2.0) unit cell containing a single benzene molecule, all coupled to the infinite zeolite solid (containing no additional benzenes). The central cell contains 192 T-atoms, 384 oxygens, 64 Na ions, in addition to the benzene, totaling 652 particles. The unit cell is cubic, with a lattice parameter of 24.848 Å.[20] Periodic boundary conditions are used throughout. Short-range interactions are cut off at 12 Å, and long-range interactions are calculated with the Ewald method.[31]

The central cell potential energy takes the form

$$V = V_Z + V_B + V_{ZB} \tag{2.1}$$

where V_Z is the zeolite frame potential, V_B is the gas phase benzene potential, and V_{ZB} is the zeolite−benzene potential. In our model V_{ZB} contains only two-body terms, whereas V_Z contains up to three-body terms and V_B up to four-body terms. In particular, we have that

$$V_Z = V_{ZCoul} + V_{Buck} + V_{Z3}$$
$$V_B = V_{H2} + V_{H3} + V_{Tor} \tag{2.2}$$

and

$$V_{ZB} = V_{ZBCoul} + V_{LJ}$$

The zeolite Coulombic energy is given by

$$V_{ZCoul} = \sum_{\text{cells}} \sum_{ij}{}' \frac{q_i q_j}{r_{ij}} \tag{2.3}$$

where the (i,j) summation avoids both double counting and self-interactions in the central cell. The zeolite framework short-range interactions are modeled with a Buckingham potential, written as

$$V_{Buck} = \sum_{i>j} [A_{ij} e^{-r_{ij}/\varrho_{ij}} - C_{ij}/r_{ij}^6] \tag{2.4}$$

All zeolite atom pairs contribute to V_{Buck} except for T−T, Na−Na, and T−Na. This exclusion is valid because the repulsive Coulombic forces preclude these species from getting close enough to affect V_{Buck} significantly. Zeolite three-body terms are included to maintain TO_4 tetrahedra. We adopt the three-body form of Catlow *et al.*,[4] given by

$$V_{Z3}' = \sum_{ijk} \frac{1}{4} A_{ijk} B_{ijk}^2 e^{-r_{ij}/\varrho_1} e^{r_{kj}/\varrho_2} \tag{2.5}$$

where

$$A_{ijk} = K_{ijk}/[2(\theta_0 - \pi)^2]$$
$$B_{ijk} = (\theta_0 - \pi)^2 - (\theta_{ijk} - \pi)^2$$

The list of 1152 faujasite three-body triplets (O_i−T_j−O_k) is stored prior to performing energy calculations. The three-body angle is given by $\cos(\theta_{ijk}) = (\vec{r}_{ij} \cdot \vec{r}_{kj})/(r_{ij} r_{kj})$.

The gas phase benzene potential terms are

$$V_{H2} = \sum_{ij} \frac{1}{2} K_{ij} [r_{ij} - r_{ij}^{(0)}]^2$$
$$V_{H3} = \sum_{ijk} \frac{1}{2} K_{ijk} [\theta_{ijk} - \theta_{ijk}^{(0)}]^2 \tag{2.6}$$
$$V_{Tor} = \sum_{ijkl} K_{ijkl} [1 - \cos(N_{ijkl} \phi_{ijkl})]$$

where lists of the 12 bond pairs (i,j), 18 angle triplets (i,j,k), and 24 dihedral quartets (i,j,k,l) are prestored. The dihedral angle is given by

$$\cos(\phi_{ijkl}) = \frac{\vec{r}_{ij} \times \vec{r}_{kj}}{|\vec{r}_{ij} \times \vec{r}_{kj}|} \cdot \frac{\vec{r}_{jk} \times \vec{r}_{lk}}{|\vec{r}_{jk} \times \vec{r}_{lk}|} \tag{2.7}$$

The host−guest interaction terms take the form

$$V_{ZBCoul} = \sum_{\text{cells}} \sum_{i \in Z} \sum_{j \in B} \frac{q_i q_j}{r_{ij}} \tag{2.8}$$

and

$$V_{LJ} = \sum_{i \in Z} \sum_{j \in B} 4\epsilon_{ij} \left[\left(\frac{\sigma_{ij}}{r_{ij}} \right)^{12} - \left(\frac{\sigma_{ij}}{r_{ij}} \right)^{6} \right] \tag{2.9}$$

The host−guest Coulombic energy is calculated with Ewald sums, taking into account the interaction of a single benzene molecule with an infinite zeolite solid. All host−guest atom

TABLE 1: Partial Charges for the Zeolite−Hydrocarbon Potential

species	partial charge	reference
Si	+2.4	28
Al	+1.4	28
T	+2.0$\bar{6}$	Si:Al = 2.0
O	−1.2	28
Na	+1.0	28
C	−0.153	15
H	+0.153	15

TABLE 2: Zeolite Short-Range Buckingham Parameters from New Fit

species	A (eV)	ϱ (Å)	C (eV Å^6)
T−O	17796.1	0.2049	135.4
O−O	1305.9	0.3594	196.1
Na−O	3542.2	0.2418	0.0

TABLE 3: Zeolite Three-Body Parameters from Catlow *et al.*

species	K (eV rad^2)	ϱ_1 (Å)	ϱ_2 (Å)	θ_0 (deg)
O−T−O	729.0189	0.3277	0.3277	109.47

TABLE 4: Gas Phase Benzene Parameters from Oie *et al.* and Catlow *et al.*

bond pair	K (eV Å^{-2})	$r^{(0)}$ (Å)
C−C	48.94	1.40
C−H	31.25	1.08
angle triplet	K (eV rad^{-2})	$\theta^{(0)}$ (deg)
C−C−C	3.39	120.0
C−C−H	3.39	120.0
dihedral quartet	K (eV)	N
C−C−C−C	0.04339	2
C−C−C−H	0.04339	2
H−C−C−H	0.04339	2

TABLE 5: Host−Guest Lennard-Jones Parameters from New Fit

species	σ (Å)	ϵ (10^{-3} eV)
O−C	3.007	7.670
O−H	2.606	5.116
Na−C	3.545	1.655
Na−H	2.944	1.255

pairs contribute to V_{LJ} except for T−C and T−H pairs. We exclude these interactions because the T-atoms are deeply embedded in the frame, making T−C and T−H distances relatively large.

The potential parameters are given in Tables 1−5. The Si and O charges in Table 1 are taken from *ab initio* calculations of Kramer *et al.*,[28] and the Al charge is determined by assuming $q_{Na} = +1$. The Si:Al ratio of 2.0 gives a T-atom charge of +2.0$\bar{6}$. The C and H charges are taken from MNDO calculations of Bull *et al.*[15] Both the zeolite and benzene three-body parameters in Tables 3 and 4, respectively, are taken from Catlow *et al.*[4] The benzene bond and torsional parameters in Table 4 are taken from Oie *et al.*[32] The zeolite short-range Buckingham parameters in Table 2 and the host−guest Lennard-Jones parameters in Table 5 result from our new fit.[19]

C. Binding Sites and Energies. As discussed above, we fit our PES to diffraction and thermochemical data for benzene in Na-Y. To test the quality of fit for the zeolite structure itself, we have relaxed Na-Y with our new PES starting from the crystallographic structure. The root mean square displacement of all zeolite atoms is 0.2 Å atom^{-1}. Thus, our zeolite PES contains a local minimum very close to the experimental structure. A more challenging test of the PES, which we have not yet attempted, is to compare the relative stabilities of different zeolite phases.[22] Future improvements for the zeolite potential are planned by fitting to additional data, such as vibrational spectra.

All energy optimizations are performed with our 36 000-line program DIZZY. The zeolite annealing sequence, called MD-DOCKER, consists of several cycles of high-temperature molecular dynamics (MD) followed by full system relaxation. The zeolite−benzene annealing algorithm adds to MD-DOCKER a very high temperature translational and orientational Monte Carlo move prior to each MD run. A typical annealing calculation consists of 10 heat−cool cycles, heating with the Monte Carlo move followed by 0.5 ps of 600 K MD. We then cool the system with the dynamic minimization algorithm LFOPC developed by Snyman,[33−35] useful for large systems in which Hessian-based methods require too much memory. Full system annealing typically requires 24 CPU hours, whereas fixed lattice annealing requires 5 CPU hours, all on an SGI Challenge workstation.

After performing 20 MD-DOCKER calculations, i.e. 200 energy minimizations, and analyzing the results with Biosym Technologies' INSIGHT,[36] we find two distinct binding sites for benzene in Na-Y, in agreement with the powder neutron diffraction results of Fitch *et al.*[20] Analogous calculations by Snurr *et al.*[37] locate 27 potential minima for benzene in silicalite, the siliceous form of ZSM-5. This illustrates differences in both the symmetry and electrostatics of the two zeolite hosts. Since silicalite has lower symmetry than Na-Y, one expects more distinct binding sites in the former. Also, since benzene is a nucleophile, the number of accessible cation types determines the number of distinct binding sites. In Na-Y, which has one such cation type (i.e. Na(II)), there are few distinct binding sites. Alternatively, since silicalite contains no cations, benzene potential minima result from the corrugation of the nonpolar silicalite frame. These minima are typically shallower and more plentiful.

We now discuss the structure and energetics of benzene sorbed in Na-Y. The zero of energy is determined as follows. First, we relax the Na-Y structure without benzene, yielding the potential energy E_Z. Second, we relax a gas phase benzene molecule, giving the potential energy E_B. Thus, $E_Z + E_B$ is the potential energy of separately optimized Na-Y and benzene. In what follows, this serves as the reference potential energy from which all other potential energies are measured.

The S_{II} and W binding geometries are shown in Figure 1. The central benzene is at the S_{II} site, 2.7 Å above Na (hidden), in agreement with the crystallographic structure.[20] The upper right benzene is at the W site, centered in the 12-ring window, 5.3 Å from the S_{II} site. We calculated site binding energies with and without lattice relaxation. With a rigid lattice we obtain $\Delta E(S_{II}) = -75$ kJ mol^{-1} and $\Delta E(W) = -50$ kJ mol^{-1}. In both cases lattice relaxation stabilizes the system by only 1 kJ mol^{-1}, indicating that such relaxation is unimportant. Also, after locating fixed lattice transition state geometries for benzene-hopping processes (*vide infra*), we allowed for lattice relaxation and find this effect to be quite small as well. Indeed, because the faujasite supercage and 12-ring window are so large relative to benzene, framework flexibility is not expected to play a major role. For these reasons, the zeolite structure including Na ions is held rigid for the remaining calculations.

The calculated binding energies agree broadly with measured heats of sorption (ΔH_{sorb}) for benzene in faujasite. In particular, the S_{II} binding energy, −75 kJ mol^{-1}, was fit to $\Delta H_{sorb} = 75$ kJ mol^{-1} for benzene in Na-Y (Si:Al = 2.43),[38] where ΔH_{sorb}

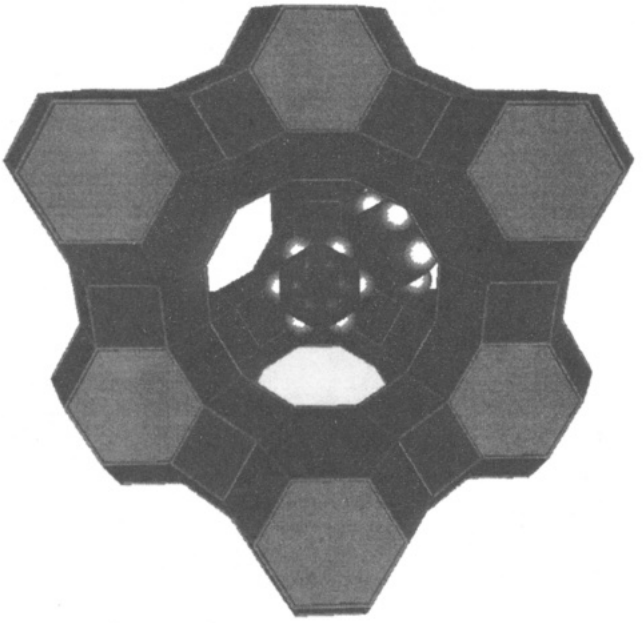

Figure 1. Binding geometries of benzene in Na-Y. Central benzene is at the S_{II} site, 2.7 Å above Na(II), with a binding energy of −75 kJ mol^{-1}. Upper right benzene is at the W site, 5.3 Å from the S_{II} benzene, with a binding energy of −50 kJ mol^{-1}.

was found to be roughly constant in the temperature range 373−523 K and was obtained by extrapolating loadings to infinite dilution. The W binding energy, −50 kJ mol^{-1}, coincides with $\Delta H_{sorb} = 55$ kJ mol^{-1} for benzene in zero-defect dealuminated Y (ZDDAY),[39] which at 300 K was found to be independent of coverage for loadings up to 22 benzenes per unit cell. In addition, quantum cluster calculations for benzene in a Na-Y 12-ring predict a W binding energy of −49.8 kJ mol^{-1},[40] in close agreement with our value. The binding energies indicate that the S_{II} population dominates over the W population at all relevant temperatures, with an equilibrium constant on the order of 10^4 at room temperature.

III. Theory of Activated Diffusion

A. Kinetic Monte Carlo. A recent spin−lattice relaxation NMR study of benzene mobility in zeolites X and Y has enabled us to estimate the time scales necessary to model diffusion in these systems.[15] The room temperature NMR diffusion coefficient for benzene in ZDDAY (i.e. siliceous Y) is $(4.5 \pm 3.3) \times 10^{-10}$ m^2 s^{-1}, while that for benzene in Na-Y (Si:Al = 1.7) is $(3.6 \pm 1.4) \times 10^{-12}$ m^2 s^{-1}. Assuming a diffusive length scale of 1 nm and the Einstein relation $R^2 = 6Dt$, we estimate that a time scale of *ca.* 400 ps is required for the siliceous system and *ca.* 50 ns for the cationic system. Bull *et al.*[15] performed a 25 ps long MD simulation of benzene in ZDDAY, revealing vigorous intracage motion at 298 K and cage-to-cage migration at 400 K. However, mobility in the cationic system is entirely too sluggish for MD, requiring instead the KMC random walk approach. We note that, in addition to calculating MD heats of sorption, Demontis *et al.*[41] attempted to use MD to model benzene diffusion in Na-Y at 326 K with a 24 ps long simulation. That the length of their simulation is too short to model diffusion is borne out by their reported diffusion coefficient, 4×10^{-9} m^2 s^{-1}, appropriate for the siliceous system, but 2−3 orders of magnitude too large for the cationic one.

We apply the KMC algorithm to benzene diffusion in Na-Y by replacing the zeolite framework with a three-dimensional lattice of S_{II} and W binding sites. Such a lattice model is known to accurately reproduce diffusive behavior when site residence times are much longer than travel times between sites.[9,42] This is indeed the case for benzene diffusion in cation-containing faujasites, as demonstrated by the two-dimensional NMR experiments of Wilhelm *et al.*[16] Connecting the S_{II} and W sites are four distinct hopping events, each with a characteristic rate coefficient: $k(S_{II}\rightarrow S_{II})$, $k(S_{II}\rightarrow W)$, $k(W\rightarrow S_{II})$, and $k(W\rightarrow W)$. The probability to make a particular hop is proportional to the associated rate coefficient. A hop is made every KMC step,[43] and the system clock is updated accordingly. This is in contrast to the standard thermal Monte Carlo procedure which has no obvious clock. The mean time elapsed before each hop is the inverse of the *total* rate coefficient to leave the originating site.[43] For example, if benzene hops from an S_{II} site, the time elapsed is

$$\Delta t(S_{II}) = \frac{1}{3[k(S_{II}\rightarrow S_{II}) + k(S_{II}\rightarrow W)]} \tag{3.1}$$

where the factor of 3 counts available target sites in the Na-Y supercage structure. Since the rate coefficients for leaving the S_{II} site are typically much smaller than those for leaving the W site, the elapsed S_{II} time is much larger than the elapsed W time. Thus, the KMC random walk algorithm efficiently models both sluggish and rapid motions in the Na-Y−benzene system.

The detailed balance among hopping processes ensures that the benzene molecule is in thermal equilibrium throughout the random walk. We obtain the diffusion coefficient from the ratio $\langle R^2(t)\rangle/6t$, where the ensemble average $\langle\cdots\rangle$ is calculated by multiple-time-step, multiple-time-origin analysis of a single random walk. In this approach, we first choose a time bin width, Δt_{bin}, usually the average residence time at the S_{II} site. For the time $t = n\Delta t_{bin}$ the mean square displacement is given by

$$\langle R^2(n\Delta t_{bin})\rangle = \frac{1}{Q(n)}{\sum_{lm}}'|\vec{r}_l - \vec{r}_m|^2 \tag{3.2}$$

where $\vec{r}_k$ is the center of mass (COM) benzene position at time t_k. The sum is restricted to those pairs (l,m) for which $t_l - t_m$ falls into the nth time bin, characterized by $n = \text{int}[(t_l - t_m)/\Delta t_{bin}]$, and $Q(n)$ is the number of such pairs. With our 4000-line program ZEOKMC, we can accurately average $\langle R^2(t)\rangle \leq 1000$ Å^2 with 16 000 KMC steps, requiring 0.5 CPU hour per temperature on the SGI Challenge workstation.

B. Rate Coefficients and Minimum Energy Paths. In the present study we estimate rate coefficients using the Arrhenius formula, in which $k \cong \nu e^{-\beta E_a}$, where ν and E_a are temperature independent. We assume that the Arrhenius prefactors $\{\nu\}$ resemble typical vibrational frequencies, on the order of 10^{13} s^{-1}. We believe these rate coefficients are sufficiently accurate for the purpose of drawing qualitative conclusions. To seek more quantitative predictions, we can apply transition state theory[44] to probe the importance of fluctuations of modes other than the reaction coordinate for determining hopping rates. Furthermore, we can apply dynamically exact flux correlation function theory,[45,46] to probe the coupling of lattice motion with sorbate relaxation from the transition state. In particular, this can indicate whether relaxation to final hopping sites is rapid relative to the vibrational period in the final site, i.e. whether transition state theory is accurate for a particular hopping process. Since the magnitude of these corrections is much smaller than the exponential effect of the Boltzmann factor, we focus our attention below on calculating activation energies.

The activation energy is the difference between the transition state energy and the initial site energy. We locate the transition state for a particular hop by following the minimum energy path

(MEP) from an initial site, through the transition state, to the final site. We calculate MEPs using a constrained optimization approach, which drags benzene from one site to another by constraining only a single component of the benzene COM, allowing all other coordinates to relax. First we define a jump vector $\vec{r}_{ab}$, pointing from the COM of the original binding site (a) to that of the target site (b). Intermediate positions along $\vec{r}_{ab}$ are defined by $\vec{r}_{ab}(\lambda) = \vec{r}_a + \lambda\vec{r}_{ab}$, where λ is a primitive reaction coordinate on the interval [0,1]. For a given λ, we define a constraint plane P_{con} (cf. holonomic constraint[47]) orthogonal to the jump vector $\vec{r}_{ab}$ and containing the point $\vec{r}_{ab}(\lambda)$. For this value of λ, we constrain the benzene COM to lie in P_{con} while relaxing all other coordinates.

We achieve this (although imperfectly) by applying a constraint potential V_{con} to the benzene COM component lying along the jump vector, where V_{con} is given by

$$V_{con} = \frac{1}{2}k_{con}\left\{[\vec{r}(t) - \vec{r}_{ab}(\lambda)] \cdot \frac{\vec{r}_{ab}}{|\vec{r}_{ab}|}\right\}^2 \qquad (3.3)$$

In eq 3.3, $\vec{r}(t)$ is the instantaneous benzene COM, and k_{con} is typically 1 eV Å^{-2}. Once a constrained MD-DOCKER annealing calculation is performed for a given λ yielding a point on the MEP, the resulting configuration is used to initiate the constrained annealing for the next value of λ. To the extent that the constraint is not perfectly enforced, a residual constraint energy contributes to the annealed system potential energy. This is subtracted from each energy along the MEP to yield the final hopping energy profile.

In addition to providing the activation energies, the MEPs also provide insight into the hopping processes. Because benzene mobility in Na-Y is too slow to be modeled by MD, we cannot actually observe benzene as it hops from site to site. Nevertheless, the MEP provides a picture of the most probable path for a particular hopping process.

The reaction coordinate used to define the abscissae in all hopping energy profiles is now defined. The goal is to condense the activities of 36 coordinates into a single reaction coordinate. We chose not to use λ, because this is too primitive and has no length scale. We wanted the reaction coordinate to contain information about benzene orientational motion along the MEP in addition to its COM motion. In what follows, we use $\mathcal{R}$ to denote the 36-dimensional benzene configuration. For the ith point on the MEP connecting stable benzene configurations $\mathcal{R}_a = \mathcal{R}_{i=0}$ and $\mathcal{R}_b = \mathcal{R}_{i=N}$, our reaction coordinate is given by $q_i = {}^1/_2[|\mathcal{R}_i - \mathcal{R}_a| - |\mathcal{R}_i - \mathcal{R}_b|]$, giving $-q_{i=0} = {}^1/_2|\mathcal{R}_a - \mathcal{R}_b| = +q_{i=N}$. The symmetry of benzene is taken into account in the definition of $|\mathcal{X} - \mathcal{Y}|$, by permuting over the atom indices to obtain the physically meaningful, shortest distance.

By using the full benzene configuration, we measure the effect of all motion—translational, rotational, and vibrational—along the MEP. The total path length, $|\mathcal{R}_a - \mathcal{R}_b|$, is generally longer than that obtained by using only COM coordinates. For example, the $S_{II} \rightarrow S_{II}$ COM jump length is 5.5 Å, whereas our full dimensional reaction coordinate path length is 12 Å. For benzene in Na-Y, this additional distance mostly reflects reorientational motion along the MEP. The reaction coordinate is also very useful for identifying early or late barriers for asymmetric hopping processes, as we demonstrate below for the $S_{II} \rightarrow W$ jump.

IV. Benzene-Hopping Paths and Energetics in Na-Y

We now discuss the results of our MEP calculations for benzene in Na-Y. In Figures 2a we present the $S_{II} \leftrightarrow S_{II}$ MEP. Our PES predicts a "cartwheel" type motion, in which benzene

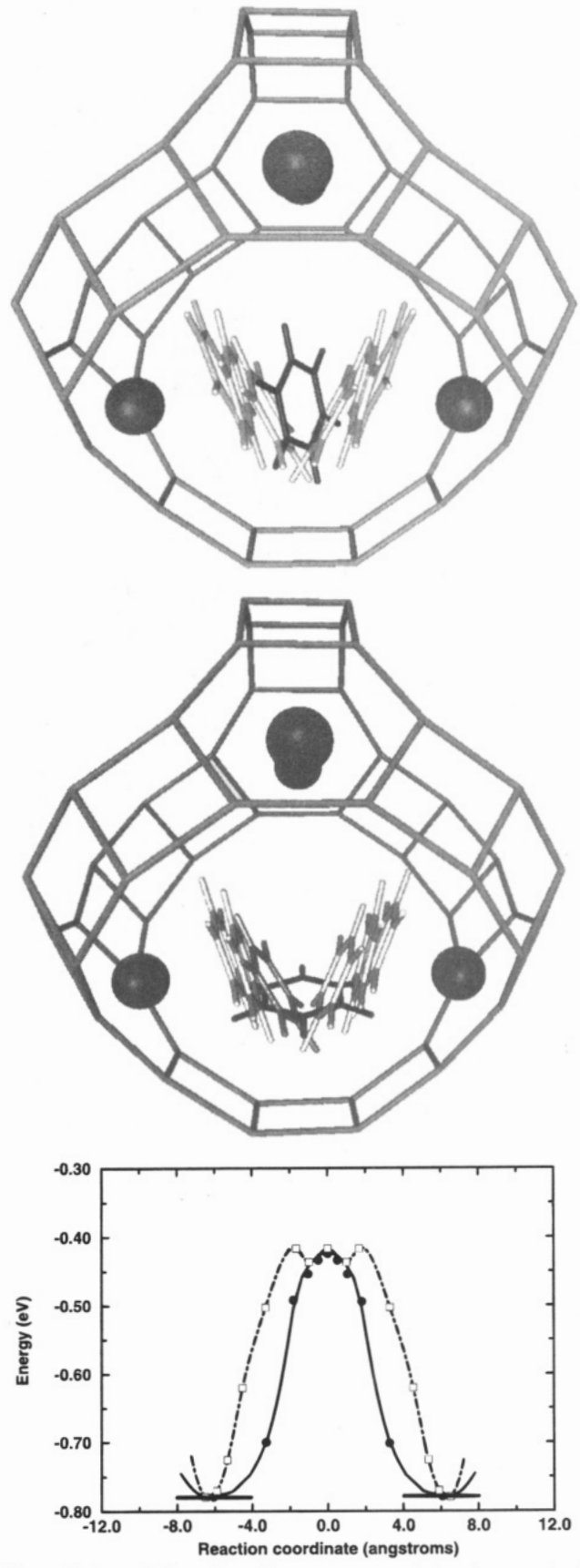

Figure 2. (a, top) $S_{II} \leftrightarrow S_{II}$ minimum energy path showing cartwheel motion, with transition state indicated in bold. (b, middle) Alternative $S_{II} \leftrightarrow S_{II}$ hopping path with skateboard motion; transition state also in bold. (c, bottom) $S_{II} \leftrightarrow S_{II}$ energetics; both paths have 35 kJ mol^{-1} activation energy. Cartwheel in solid, skateboard in dashes.

remains roughly orthogonal to intermediate 4-rings. This result is surprising, since we envisioned a "skateboard" type motion

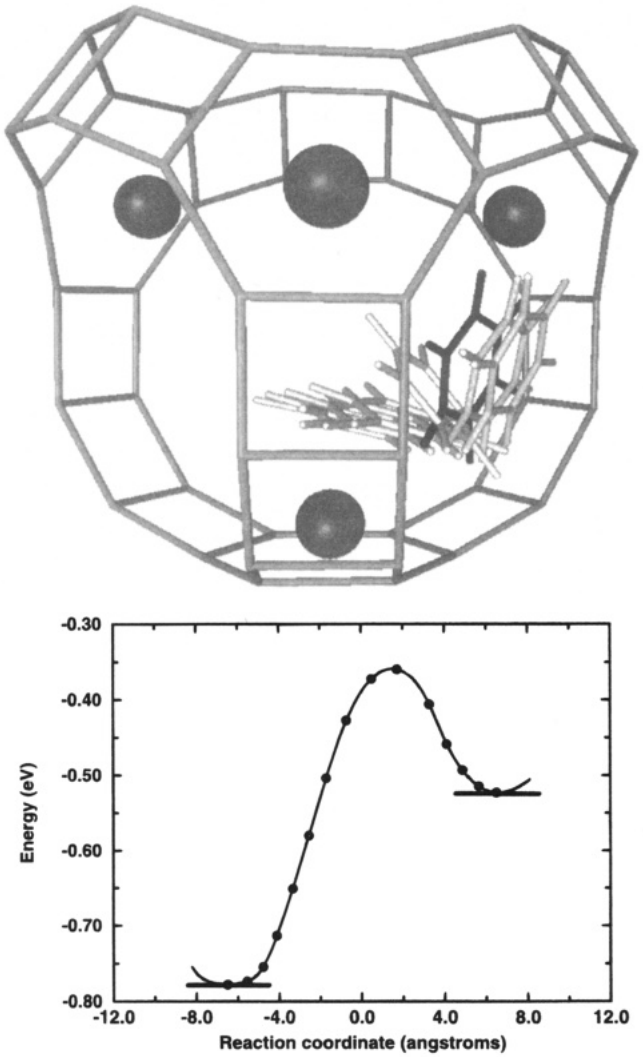

Figure 3. (a, top) $S_{II} \leftrightarrow W$ minimum energy path showing cartwheel motion, with transition state indicated in bold. (b, bottom) $S_{II} \leftrightarrow W$ energetics; 41 kJ mol^{-1} largest barrier in KMC simulation.

in which benzene remains parallel to intermediate 4-rings. Indeed, we located an alternate $S_{II} \leftrightarrow S_{II}$ hopping path (not the MEP) shown in Figure 2b, which demonstrates the skateboard mechanism. The relative energetics of these two paths are shown in Figure 2c, with cartwheel in solid and skateboard in dashes. Although the skateboard energies are systematically higher than the cartwheel energies, the overall activation energies are both 35 kJ mol^{-1}. Since we assume the Arrhenius rate coefficient formula, both paths are equally important.

A KMC simulation using only the $S_{II} \leftrightarrow S_{II}$ hopping process would model intracage mobility of benzene in Na-Y. To examine intercage migration, and hence long length scale diffusion, we calculated the $S_{II} \leftrightarrow W$ MEP shown in Figure 3a. This MEP also demonstrates the cartwheel mechanism observed for the $S_{II} \leftrightarrow S_{II}$ MEP. The energy along the $S_{II} \leftrightarrow W$ path, shown in Figure 3b, has a minimum at the W site and a 41 kJ mol^{-1} activation barrier for the $S_{II} \rightarrow W$ process. The excess activation energy of $S_{II} \rightarrow W$ relative to $S_{II} \rightarrow S_{II}$ arises because the $S_{II} \rightarrow W$ transition state is less strongly bound to intermediate 4-rings. Figure 3b also predicts a late $S_{II} \rightarrow W$ transition state, in accord with Hammond's postulate; that is, the transition state between a stable state (the S_{II} site) and a high-energy reactive intermediate (the W site) more closely resembles the reactive intermediate.

A direct $W \leftrightarrow W$ hopping event is also possible, analogous to interstitial diffusion in dense solids. This process gains importance at higher benzene loadings, e.g. ~4 per supercage, as all S_{II} sites become occupied with benzene. We focus on benzene in Na-Y at infinite dilution and, hence, do not discuss the $W \leftrightarrow W$ hop further, although for completeness it is included in our KMC simulation.

TABLE 6: Hopping Activation Energies and Hypothetical Arrhenius Prefactors for Benzene in Na−Y[a]

jump	activation energy (kJ mol^{-1})	Arrhenius prefactor (s^{-1})
$S_{II} \rightarrow S_{II}$	35	10^{13}
$S_{II} \rightarrow W$	41	10^{13}
$W \rightarrow S_{II}$	16	$10^{13}-10^{14}$
$W \rightarrow W$	18	$10^{13}-10^{11}$

[a] Our PES predicts that $S_{II} \rightarrow W$ is rate limiting and that leaving the W site is relatively facile. Sensitivity to Arrhenius prefactors for leaving the W site was tested by using the two sets shown.

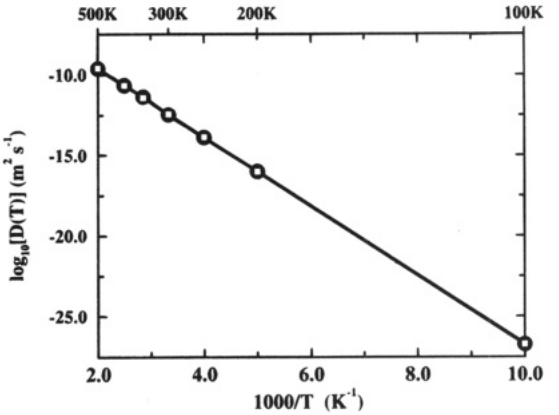

Figure 4. Arrhenius plot of diffusion coefficients. Filled circles: all $\nu = 10^{13}$ s^{-1}. Open squares: $\nu(S_{II} \rightarrow S_{II}) = \nu(S_{II} \rightarrow W) = 10^{13}$ s^{-1}, $\nu(W \rightarrow S_{II}) = 10^{14}$ s^{-1}, $\nu(W \rightarrow W) = 10^{11}$ s^{-1}. Two prefactor sets give the same diffusion coefficients. Arrhenius fit gives $E_a = 41$ kJ mol^{-1}, exactly the $S_{II} \rightarrow W$ activation energy, and $D_0 = 4.8 \times 10^{-6}$ m^2 s^{-1}.

We summarize the hopping energies and hypothetical Arrhenius prefactors in Table 6. We note that leaving the W site is much more facile than leaving the S_{II} site. Indeed, the predicted 300 K residence time at the W site is *ca.* 6 ps; whereas that for the S_{II} site is *ca.* 34 ns. Various mobility measurements for this and closely related systems report activation energies ranging from 14 to 27 kJ mol^{-1}.[15] Since our activation energies are systematically larger then those measured, further PES refinement may be required. Nevertheless, with different types of hopping processes contributing to intercage diffusion, the KMC simulation will determine which hopping process, if any, controls the diffusivity.

V. Analysis of Benene Mobility in Na-Y

A. Benzene Diffusion. We have modeled the mobility of benzene in Na-Y over the temperature range 100−500 K with the two sets of Arrhenius prefactors in Table 6. In Figure 4 we show an Arrhenius plot of the resulting diffusion coefficients, i.e. $\log_{10}(D)$ vs $1000/T$. Several points can be made. First, the two sets of Arrhenius prefactors give virtually identical diffusion coefficients. This indicates that the details of leaving the W site are unimportant (at infinite dilution), since the process is so facile. Second, the diffusion coefficients fit the Arrhenius form over the entire 17 orders of magnitude range. We discuss below when one would expect non-Arrhenius behavior. Third, the apparent activation energy is 41 kJ mol^{-1}, exactly the $S_{II} \rightarrow W$ activation energy. Although one might expect this simply because $E_a(S_{II} \rightarrow W)$ is the largest activation energy in the KMC simulation, this actually results from simulating long-range diffusion, in which escape from the cage *via* the $S_{II} \rightarrow W$ hop

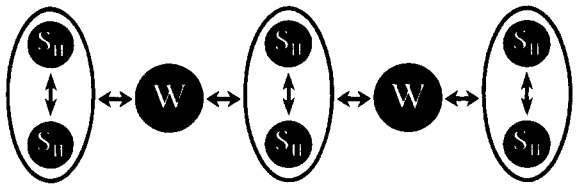

Figure 5. Schematic depiction of benzene motion through Na-Y, demonstrating that the serial $S_{II} \rightarrow W$ process is required for long-range motion and, hence, controls it, whereas the parallel $S_{II} \rightarrow S_{II}$ hop does not contribute to diffusion and, hence, cannot be detected by a diffusion measurement.

is a necessary step. Indeed, even if $E_a(S_{II} \rightarrow S_{II}) > E_a(S_{II} \rightarrow W)$, the apparent activation energy for diffusion would still be $E_a(S_{II} \rightarrow W)$, since the $S_{II} \rightarrow S_{II}$ jump is *not required* for long-range motion. We demonstrate this point schematically in Figure 5, in which the required serial process is the $S_{II} \rightarrow W$ hop, whereas the optional parallel process is the $S_{II} \rightarrow S_{II}$ jump. As such, our calculations suggest that activation energies from long length scale diffusion measurements, e.g. pulsed field gradient NMR, should be interpreted as site-to-window activation energies.

We now compare our calculated barriers with those from theoretical and experimental studies. Klein *et al.*[18] use a similar molecular mechanics PES to calculate binding sites and hopping activation energies for aromatics in Na-Y (Si:Al = 3.0). Using smaller partial charges for the zeolite (i.e. $q_T = +1.2$, $q_O = -0.7$, and $q_{Na} = +0.8$), they obtain the following very similar barriers for benzene mobility: $E_a(S_{II} \rightarrow S_{II}) = 30$ kJ mol^{-1} and $E_a(S_{II} \rightarrow W) = 43$ kJ mol^{-1}.[18] This indicates that the barriers are somewhat insensitive to the underlying charge set. Experimental diffusion activation energies for this and closely related systems fall in the range 14–27 kJ mol^{-1}.[15] Although our predicted apparent activation energy of 41 kJ mol^{-1} appears to be too large by a factor of 2, we argue below in section VB that our predicted value for $E_a(S_{II} \rightarrow S_{II})$ may only be too large by approximately 10 kJ mol^{-1}, which is roughly the spread in measured heats of sorption for this class of systems.[48] Performing quantum cluster calculations on the stable and transition state structures will hopefully improve the accuracy of our theoretical barriers. Nevertheless, we have demonstrated that it is indeed possible to extract qualitatively reasonable activation barriers from a PES fitted exclusively to stable state data.

The Arrhenius plot in Figure 4 also yields an overall diffusion prefactor $D_0 = 4.8 \times 10^{-6}$ m^2 s^{-1}. To fully understand the mobility, we decompose this into an effective hopping length b_e and attempt frequency ν_e,[42] such that $D_0 = b_e^2 \nu_e$. A natural length scale to choose is the cage-to-cage length $b_e = 11$ Å, resulting in an attempt frequency $\nu_e = 3.8 \times 10^{12}$ s^{-1} $\cong$ $^1/_3 \times 10^{13}$ s^{-1}. This effective cage-to-cage frequency can be understood with the following analysis.

By choosing b_e as the cage-to-cage length, we imagine that—although hops really take place among S_{II} and W sites—long-range motion involves hops from one "cage site" to a neighboring "cage site". As such, all the S_{II} and W site structure within a cage becomes the internal structure of the cage site. Associated with this cage-to-cage hopping process is the rate coefficient k_e. It can be shown[49] that the diffusion coefficient for benzene in faujasite can be written as $D = {}^1/_6 k_e b_e^2$. We give a brief proof below; the detailed proof is given in ref 49. After N random jumps of length b_e on the diamond lattice of faujasite supercages, the mean square displacement is given by

$$\begin{aligned} \langle R^2(N) \rangle &= \left\langle \left| \sum_{i=1}^{N} \boldsymbol{l}_i \right|^2 \right\rangle \\ &= \left\langle \sum_{i=1}^{N} |\boldsymbol{l}_i|^2 \right\rangle + \left\langle \sum_{i \neq j} \boldsymbol{l}_i^T \cdot \boldsymbol{l}_j \right\rangle \\ &= \left\langle \sum_{i=1}^{N} b_e^2 \right\rangle = N b_e^2 = k_e t b_e^2 = 6Dt \end{aligned} \tag{5.1}$$

The third equality results because jumps are uncorrelated, and the final equality establishes the desired result. Furthermore, we have found from independent KMC calculations that the cage-to-cage rate coefficient is well fit by $k_e = {}^1/_2 \times 4 \times k(S_{II} \rightarrow W)$. The factor of 1/2 accounts for randomizing in the W site, which halves the probability to leave the cage. The factor of 4 accounts for the four ways to leave the supercage through one of the four windows. From these observations we deduce that $D_0 = ({}^1/_6 \times 4 \times {}^1/_2)\, b_e^2 \nu(S_{II} \rightarrow W)$, which gives $\nu_e = {}^1/_3 \times 10^{13}$ s^{-1}, in quantitative agreement with the KMC simulation results. Thus, we have demonstrated how the diffusion prefactor can be constructed from fundamental length and time scales. Conversely, it should be possible to decompose a measured diffusion prefactor into these basic quantities, yielding insight into the microscopic processes that control diffusion in zeolites.

Experimental Arrhenius prefactors for this and closely related systems fall in the range 1.2×10^{-10} to 1.5×10^{-7} m^2 s^{-1}.[15] The geometric average of the actual values tabulated in ref 15 gives $\langle D_0 \rangle = 8.9 \times 10^{-9}$ m^2 s^{-1}, as compared with our theoretical value, 4.8×10^{-6} m^2 s^{-1}. In principle, this discrepancy results exclusively from our posited microscopic prefactor $\nu = 10^{13}$ s^{-1}. Indeed, the experimental diffusion prefactors suggest a microscopic prefactor at least 2 orders of magnitude smaller, on the order of 10^{10}–10^{11} s^{-1}. We are presently calculating prefactors for several important microscopic hopping processes to compare with these experimental estimates.

B. Benzene Reorientation. Two questions naturally arise from the above analysis. First, having found that the $S_{II} \rightarrow W$ hop rate controls long-range transport, one may ask what physical situation would be controlled by the intracage, $S_{II} \rightarrow S_{II}$ hopping process? Second, having found strictly Arrhenius behavior for $D(T)$, one may ask what physical situation would generate non-Arrhenius behavior, even when the underlying rate coefficients satisfy the Arrhenius form? The answers to these questions are both related to orientational dynamics of, for example, benzene in Na-Y.

We imagine an experiment, e.g. spin–lattice relaxation NMR, which can measure the rate of benzene orientational randomization, resulting from the reorientation of the benzene plane during its random walk. This is interesting because both $S_{II} \rightarrow S_{II}$ and $S_{II} \rightarrow W$ hops contribute to reorientation, whereas only the latter hop contributes to diffusion. Assuming that $k(S_{II} \rightarrow S_{II})$ and $k(S_{II} \rightarrow W)$ control the orientational dynamics, and that they both obey the Arrhenius formula, there are six possibilities for the relative magnitudes of the four kinetic parameters ($E_a(S_{II} \rightarrow S_{II})$, $\nu(S_{II} \rightarrow S_{II})$; $E_a(S_{II} \rightarrow W)$, $\nu(S_{II} \rightarrow W)$). These are summarized in Table 7 along with the Arrhenius parameters (if applicable) of the overall, predicted randomization rate; we focus on sets 3, 4, and 6. Parameter set 3 corresponds to the results from our force field calculations for benzene in Na-Y. Thus, we predict that the NMR experiments of Bull *et al.*[15] are indeed observing intracage hopping processes, their data providing a direct probe of the $S_{II} \rightarrow S_{II}$ hopping rate coefficient. This suggests the more

TABLE 7: Six Possibilities for relative Magnitudes of the Four Kinetic Parameters ($E_S \equiv E_a(S_{II} \rightarrow S_{II})$, $\nu_S \equiv \nu(S_{II} \rightarrow S_{II})$; $E_W \equiv E_a(S_{II} \rightarrow W)$, $\nu_W \equiv \nu(S_{II} \rightarrow W)$) Which Control the Orientational Randomization Rate, the Arrhenius Parameters of Which Are Predicted in Columns 3 and 4[a]

input barriers	input prefactors	resulting barrier	resulting prefactor
(1) $E_S = E_W$	$\nu_S \leq \nu_W$	E_W	ν_W
(2) $E_S = E_W$	$\nu_S > \nu_W$	E_S	ν_S
(3) $E_S < E_W$	$\nu_S \geq \nu_W$	E_S	ν_S
(4) $E_S < E_W$	$\nu_S < \nu_W$	NA	NA
(5) $E_S > E_W$	$\nu_S \leq \nu_W$	E_W	ν_W
(6) $E_S > E_W$	$\nu_S > \nu_W$	NA	NA

[a] Set 3 corresponds to our Na-Y−benzene model. Sets 4 and 6 give rise to non-Arrhenius behavior, for which specifying overall Arrhenius parameters is not applicable (NA).

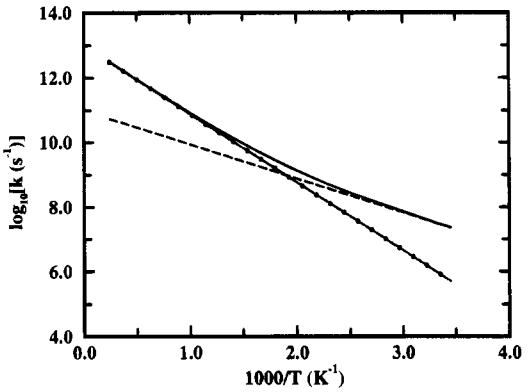

Figure 6. Temperature dependence of sample $S_{II} \rightarrow S_{II}$ and $S_{II} \rightarrow W$ rate coefficients satisfying set 4 in Table 7 plotted using kinetic parameters ($E_a(S_{II} \rightarrow S_{II})$ = 20 kJ mol^{-1}, $\nu(S_{II} \rightarrow S_{II})$ = 10^{11} s^{-1}; $E_a(S_{II} \rightarrow W)$ = 41 kJ mol^{-1}, $\nu(S_{II} \rightarrow W)$ = 10^{13} s^{-1}). At low temperatures the $S_{II} \rightarrow S_{II}$ hop (dashes) gives faster reorientation; at higher temperatures the $S_{II} \rightarrow W$ process (dots) dominates. Overall randomization rate k_{tot} (solid) displays clear non-Arrhenius behavior. Arrhenius fit to k_{tot} gives E_a = 31 kJ mol^{-1} and prefactor $\nu = 3.6 \times 10^{12}$ s^{-1}.

favorable comparison of their 24 kJ mol^{-1} apparent activation energy and our $E_a(S_{II} \rightarrow S_{II})$ = 35 kJ mol^{-1}.

Parameter sets 4 and 6 demonstrate physical situations where we expect non-Arrhenius behavior. We focus on set 4, since this involves activation energies in accord with our force field calculations. (Parameter set 6 is the same as 4 with all inequalities reversed and, as such, contains no new physics.) The temperature dependence of sample $S_{II} \rightarrow S_{II}$ and $S_{II} \rightarrow W$ rate coefficients satisfying set 4 is plotted in Figure 6, using the kinetic parameters ($E_a(S_{II} \rightarrow S_{II})$ = 20 kJ mol^{-1}, $\nu(S_{II} \rightarrow S_{II})$ = 10^{11} s^{-1}; $E_a(S_{II} \rightarrow W)$ = 41 kJ mol^{-1}, $\nu(S_{II} \rightarrow W)$ = 10^{13} s^{-1}). At temperatures lower than *ca.* 530 K, the $S_{II} \rightarrow S_{II}$ hop (dashes) is the more facile mechanism for orientational randomization, whereas at higher temperatures the $S_{II} \rightarrow W$ process (dots) dominates. The overall randomization rate k_{tot} (solid), estimated by $k(S_{II} \rightarrow S_{II}) + k(S_{II} \rightarrow W)$, displays clear non-Arrhenius behavior in Figure 6. Indeed, an Arrhenius fit to k_{tot} gives the activation energy E_a = 31 kJ mol^{-1} and the prefactor $\nu = 3.6 \times 10^{12}$ s^{-1}, neither corresponding to any of the input microscopic parameters. We are presently calculating the prefactors for these two hop processes, in addition to the relevant orientational correlation function, to determine if non-Arrhenius orientational randomization is actually predicted.

VI. Conclusions

We have modeled benzene diffusion in Na-Y zeolite (Si:Al = 2.0) over the temperature range 100−500 K. An Arrhenius fit yields the apparent activation energy E_a = 41 kJ mol^{-1} and the prefactor $D_0 = 4.8 \times 10^{-6}$ m^2 s^{-1}. This work represents the first long length scale simulation of diffusion in cation-containing zeolites. We utilize the kinetic Monte Carlo random walk model, assuming uncorrelated hops among S_{II} and W sites. Activation energies are derived from a new zeolite−hydrocarbon potential energy surface (PES), yielding $E_a(S_{II} \rightarrow S_{II})$ = 35 kJ mol^{-1}, $E_a(S_{II} \rightarrow W)$ = 41 kJ mol^{-1}, $E_a(W \rightarrow S_{II})$ = 16 kJ mol^{-1}, and $E_a(W \rightarrow W)$ = 18 kJ mol^{-1}. Minimum energy paths from the new PES demonstrate cartwheel ($S_{II} \rightarrow S_{II}$, $S_{II} \rightarrow W$) and skateboard ($S_{II} \rightarrow S_{II}$, $W \rightarrow W$) hopping mechanisms for benzene in Na-Y. Cage-to-cage analysis of the random walk indicates that the diffusion coefficient can be constructed from fundamental energy, length, and time scales. In particular, we suggest that experimentally determined activation energies and prefactors for long length scale diffusion refer to site-to-window hopping processes. We predict that measurement of benzene orientational randomization can probe activation energies and prefactors for short length scale, intracage motion and may detect non-Arrhenius temperature dependence of the randomization rate. We are implementing this theoretical framework to study the concentration dependence of benzene diffusion in Na-Y, in addition to diffusion in acidic zeolites.

Acknowledgment. We thank Dr. Shudun Liu for technical assistance with the Monte Carlo simulations, and the referees for very helpful suggestions. S.M.A. gratefully acknowledges support from a National Science Foundation postdoctoral fellowship, CHE-9403159, awarded in 1994. N.J.H. and A.K.C. thank Los Alamos National Laboratory and Biosym Technologies for financial support. H.I.M. acknowledges the NSF and the Office of Naval Research for funding. This work was partially funded by the UCSB-MRL, which is supported by the NSF under Award No. DMR-9123048.

References and Notes

(1) Catlow, C. R. A.; Price, G. D. *Nature* **1990**, *347*, 243.
(2) Smit, B.; Siepmann, J. I. *Science* **1994**, *264*, 1118.
(3) Yashonath, S.; Thomas, J. M.; Nowak, A. K.; Cheetham, A. K. *Nature* **1988**, *331*, 601.
(4) Catlow, C. R. A.; Freeman, C. M.; Vessal, B.; Tomlinson, S. M.; Leslie, M. *J. Chem. Soc., Faraday Trans.* **1991**, *87*, 1947.
(5) Sauer, J. *Nature* **1993**, *363*, 493.
(6) Kramer, G. J.; van Santen, R. A.; Emeis, C. A.; Nowak, A. K. *Nature* **1993**, *363*, 529.
(7) Metiu, H. I.; Lu, Y. T.; Zhang, Z. Y. *Science* **1992**, *255*, 1088.
(8) Fichthorn, K. A.; Weinberg, W. H. *J. Chem. Phys.* **1991**, *95*, 1090.
(9) June, R. L.; Bell, A. T.; Theodorou, D. N. *J. Phys. Chem.* **1991**, *95*, 8866.
(10) Jameson, C. J.; Jameson, A. K.; Gerald, R., II; de Dios, A. C. *J. Chem. Phys.* **1992**, *96*, 1676.
(11) Jameson, C. J.; Jameson, A. K.; Lin, H.-M.; Baello, B. I. *J. Chem. Phys.* **1994**, *100*, 5977.
(12) Yashonath, S. *J. Phys. Chem.* **1991**, *95*, 5877.
(13) Yashonath, S.; Santikary, P. *J. Phys. Chem.* **1993**, *97*, 3849.
(14) Heink, W.; Kärger, J.; Pfeifer, H.; Stallmach, F. *J. Am. Chem. Soc.* **1990**, *112*, 2175.
(15) Bull, L. M.; Henson, N. J.; Cheetham, A. K.; Newsam, J. M.; Heyes, S. J. *J. Phys. Chem.* **1993**, *97*, 11776.
(16) Wilhelm, M.; Firouzi, A.; Favre, D. E.; Bull, L. M.; Schaefer, D. J.; Chmelka, B. F. *J. Am. Chem. Soc.* **1995**, *117*, 2923.
(17) Uytterhöven, L.; Dompas, D.; Mortier, W. J. *J. Chem. Soc., Faraday Trans.* **1992**, *88*, 2753.
(18) Klein, H.; Kirschhock, C.; Fuess, H. *J. Phys. Chem.* **1994**, *98*, 12345.
(19) Henson, N. J.; Auerbach, S. M.; Metiu, H. I.; Cheetham, A. K. In preparation.
(20) Fitch, A. N.; Jobic, H.; Renouprez, A. *J. Phys. Chem.* **1986**, *90*, 1311.
(21) Jackson, R. A.; Catlow, C. R. A. *Mol. Simul.* **1988**, *1*, 207.
(22) Henson, N. J.; Cheetham, A. K.; Gale, J. D. *Chem. Mater.* **1994**, *6*, 1647.
(23) Schröder, K.-P.; Sauer, J.; Leslie, M.; Catlow, C. R. A.; Thomas, J. M. *Chem. Phys. Lett.* **1992**, *188*, 320.
(24) George, A. R.; Catlow, C. R. A.; Thomas, J. M. *J. Solid State Chem.* **1993**, *104*, 6.
(25) Brennan, D.; Bell, R. G.; Catlow, C. R. A.; Jackson, R. A. *Zeolites* **1994**, *14*, 650.

(26) Jentys, A.; Catlow, C. R. A. *Catal. Lett.* **1993**, *22*, 251.
(27) Sauer, J. *Chem. Rev.* **1989**, *89*, 199.
(28) Kramer, G. J.; Farragher, N. P.; van Beest, B. W. H.; van Santen, R. A. *Phys. Rev. B* **1991**, *43*, 5068.
(29) Alfredsson, V.; Terasaki, O.; Blum, Z.; Bovin, J. O. *Zeolites* **1995**, *15*, 111.
(30) Bull, L. M. Ph.D. Thesis, Oxford University, 1993.
(31) Allen, M. F.; Tildesley, D. J. *Computer Simulation of Liquids*; Oxford Science Publications: Oxford, 1987.
(32) Oie, T.; Maggiora, G. M.; Christoffersen, R.; Duchamp, D. D. *Int. Quantum Chem., Quantum Biol. Supp.* **1981**, *1*, 1.
(33) Snyman, J. A. *Appl. Math. Model.* **1982**, *6*, 449.
(34) Snyman, J. A. *Appl. Math. Model.* **1983**, *7*, 216.
(35) Snyman, J. A. *Comput. Math. Appl.* **1989**, *17*, 1369.
(36) *InsightII User Guide, version 2.3.0*, San Diego: Biosym Technologies, 1994.
(37) Snurr, R. Q.; Bell, A. T.; Theodorou, D. N. *J. Phys. Chem.* **1994**, *98*, 11948.
(38) Barthomeuf, D.; Ha, B. H. *J. Chem. Soc., Faraday Trans.* **1973**, *69*, 2147.
(39) Henson, N. J.; Cheetham, A. K.; Stockenhuber, M.; Lercher, J. A. In preparation.
(40) O'Malley, P. J.; Braithwaite, C. J. *Zeolites* **1995**, *15*, 198.
(41) Demontis, P.; Yashonath, S.; Klein, M. L. *J. Phys. Chem.* **1989**, *93*, 5016.
(42) Gomer, R. *Rep. Prog. Phys.* **1990**, *53*, 917.
(43) Maksym, P. *Semicond. Sci. Technol.* **1988**, *3*, 594.
(44) Pechukas, P. In *Dynamics of Molecular Collisions*; Miller, W. H., Ed.; Plenum: New York, 1976; Vol. B, 269.
(45) Chandler, D. *J. Chem. Phys.* **1978**, *68*, 2959.
(46) Zhang, Z. Y.; Haug, K.; Metiu, H. I. *J. Chem. Phys.* **1990**, *93*, 3614.
(47) Goldstein, H. *Classical Mechanics*; Addision-Wesley: Reading, MA, 1980.
(48) Henson, N. J. Ph.D. Thesis, Oxford University, 1995.
(49) Auerbach, S. M.; Henson, N. J.; Cheetham, A. K.; Metiu, H. I. In preparation.

JP9500549